

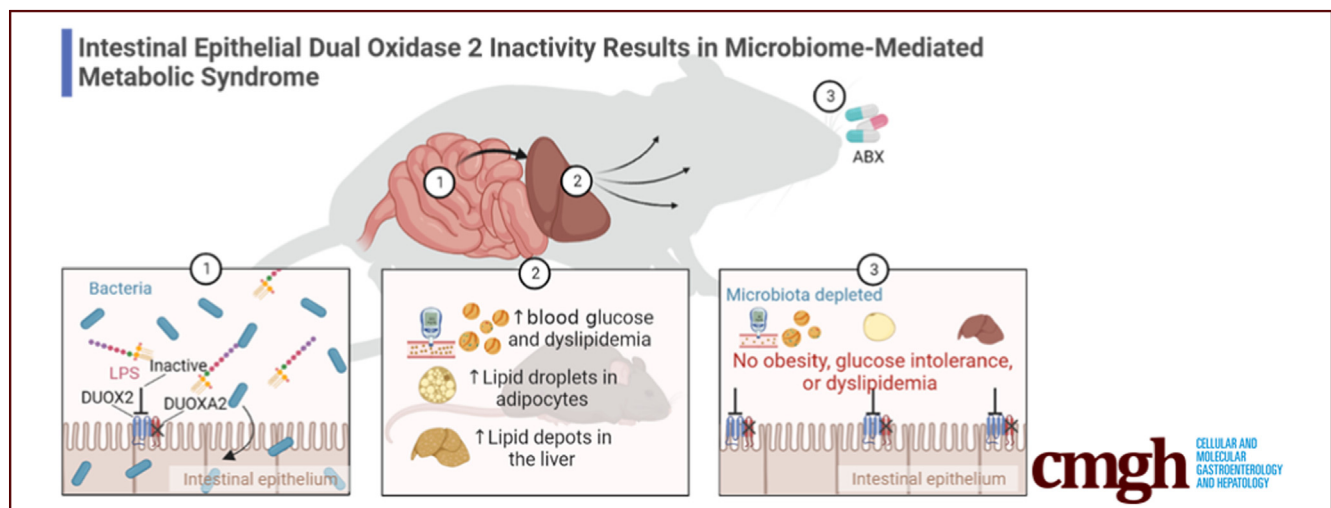
ORIGINAL RESEARCH

Intestinal Epithelial Inactivity of Dual Oxidase 2 Results in Microbiome-Mediated Metabolic Syndrome



Hajar Hazime,^{1,2,*} G. Michelle Ducasa,^{1,*} Ana M. Santander,¹ Nivis Brito,¹ Eddy E. González,¹ Yuguang Ban,³ Jonathan Kaunitz,^{4,5} Yasutada Akiba,^{4,5} Irina Fernández,¹ Juan F. Burgueño,^{1,§} and Maria T. Abreu^{1,2,§}

¹Division of Gastroenterology, Department of Medicine, University of Miami–Miller School of Medicine, Miami, Florida; ²Department of Microbiology and Immunology, University of Miami–Miller School of Medicine, Miami, Florida; ³Biostatistics and Bioinformatics Shared Resource, Sylvester Comprehensive Cancer Center, University of Miami–Miller School of Medicine, Miami, Florida; ⁴Medical Service and Research Services, VA Greater Los Angeles Healthcare System, Los Angeles, California; and ⁵Medical Service, Department of Medicine, David Geffen School of Medicine, University of California Los Angeles, Los Angeles, California



SUMMARY

Functional deficiency in intestinal epithelial dual oxidase 2 has systemic consequences. The absence of intestinal epithelial dual oxidase 2 promotes the development of metabolic syndrome in a microbiome-dependent manner.

BACKGROUND & AIMS: Metabolic syndrome (MetS) is characterized by obesity, glucose intolerance, and hepatic steatosis. Alterations in the gut microbiome play important roles in the development of MetS. However, the mechanisms by which this occurs are poorly understood. Dual oxidase 2 (DUOX2) is an antimicrobial reduced nicotinamide adenine dinucleotide phosphate oxidase expressed in the gut epithelium. Here, we posit that epithelial DUOX2 activity provides a mechanistic link between the gut microbiome and the development of MetS.

METHODS: Mice carrying an intestinal epithelial-specific deletion of dual oxidase maturation factor 1/2 (DA IEC-KO), and wild-type littermates were fed a standard diet and killed at 24 weeks.

Metabolic alterations were determined by glucose tolerance, lipid tests, and body and organ weight measurements. DUOX2 activity was determined by Amplex Red. Intestinal permeability was determined by fluorescein isothiocyanate–dextran, microbial translocation assessments, and portal vein lipopolysaccharide measurements. Metagenomic analysis of the stool microbiome was performed. The role of the microbiome was assessed in antibiotic-treated mice.

RESULTS: DA IEC-KO males showed increased body and organ weights accompanied by glucose intolerance and increased plasma lipid and liver enzyme levels, and increased adiposity in the liver and adipose tissue. Expression of F4/80, CD68, uncoupling protein 1, carbohydrate response element binding protein, leptin, and adiponectin was altered in the liver and adipose tissue of DA IEC-KO males. DA IEC-KO males produced less epithelial H₂O₂, had altered relative abundance of *Akkermansia* and *Lachnospiraceae* in stool, and showed increased portal vein lipopolysaccharides and intestinal permeability. Females were protected from barrier defects and MetS, despite producing less H₂O₂. Antibiotic depletion abrogated all MetS phenotypes observed.

CONCLUSIONS: Intestinal epithelial inactivity of DUOX2 promotes MetS in a microbiome-dependent manner. (*Cell Mol Gastroenterol Hepatol* 2023;16:557–572; <https://doi.org/10.1016/j.jcmgh.2023.06.009>)

Keywords: Reactive Oxygen Species; Dyslipidemia; Intestinal Barrier Function; Dysbiosis.

Metabolic syndrome (MetS) is characterized by the co-existence of a cluster of conditions that increase the risk of mortality, including obesity, dyslipidemia, glucose intolerance, and hepatic steatosis.^{1,2} Because of the increase in health complications related to MetS,^{3,4} research efforts are aimed at better understanding the underlying mechanisms contributing to the development of this condition. The pathogenesis of MetS is complex and involves both extrinsic (diet and environment) and intrinsic (genetic) factors that ultimately culminate in the presence of chronic low-grade inflammation, which is a key hallmark of this condition.⁵ As a result, pinpointing triggers for systemic chronic inflammation, and understanding the mechanism by which it could lead to MetS, remains a challenge.

Gut dysbiosis, defined as an imbalance in microbial composition or function, plays central roles in the development of chronic inflammation.^{6–8} In recent years, the gut microbiome has emerged as a key player involved in MetS.^{9–11} Indeed, mice raised in germ-free conditions are protected from diet-induced obesity and insulin resistance.^{12,13} Furthermore, the microbiota of obese patients and mice has been shown to be sufficient to transfer the susceptibility to obesity and MetS in gnotobiotic mice.^{14,15} To date, a dysbiotic profile specific to MetS is hard to define. However, observational studies in patients have shown trends at the phylum level.¹⁶ Notably, interventional approaches aimed at reversing MetS by modulating the microbiome, such as supplementation with *Akkermansia muciniphila*, resulted in some early success in a recent double-blinded, placebo-controlled study.¹⁷ On the host side, however, the mechanism by which dysbiosis leads to chronic inflammation and MetS is poorly defined.

The intestinal epithelium modulates host-microbiome interactions by balancing immunity and tolerance against luminal bacteria. Microbial recognition in the intestinal epithelium depends on pattern recognition receptors, including Toll-like receptors (TLRs).¹⁸ Mice lacking epithelial-specific TLR4¹⁹ and TLR5²⁰ develop obesity and a dysregulated metabolic profile, highlighting a link between dysregulated epithelial signaling and MetS. Interestingly, we recently showed that epithelial TLR4 signaling induces the release of reactive oxygen species (ROS) by means of its downstream effector, the reduced nicotinamide adenine dinucleotide phosphate oxidase, dual oxidase 2 (DUOX2).²¹ DUOX2 is induced by inflammatory cytokines and dysbiosis,^{22,23} and modulates microbial colonization of the mucosa in mice.²⁴ Indeed, loss-of-function mutations in DUOX2 have been associated with the development of pathologies such as inflammatory bowel disease (IBD)^{25,26} and very early onset IBD.^{24,27} Notably, IBDs also are characterized by

dysbiosis and chronic inflammation, suggesting common pathways in the development of these diseases. Therefore, we set out to investigate the relationship between impaired epithelial barrier function and the development of MetS by focusing on DUOX2 deficiency as a mechanistic link.

In the present study, we used mice with an intestinal epithelial-specific deletion of the DUOX2 partner proteins and maturation factors (DUOXA1/2), to show that the subsequent loss of DUOX2 enzymatic activity in the gut is enough to induce MetS. Specifically, mice with an intestinal epithelial knockout of DUOXA1/2 (DA IEC-KO) develop obesity, glucose intolerance, increased plasma lipid levels, and accumulation of lipids in the liver. We also showed that this phenotype is associated with low-grade inflammation, dysbiosis, altered gut permeability, and increased portal vein (PV) lipopolysaccharide (LPS) levels and bacterial translocation to the liver and adipose tissue. Lastly, we showed that DUOX2 deficiency alters the microbiome, and that the microbiota is necessary to induce obesity and MetS in our model. Our results support the notion that functional changes in DUOX2 activity in the intestine cause increased intestinal permeability and serve as a trigger for chronic inflammation and MetS.


Results

Intestinal Epithelial Deficiency of DUOX2 Leads to Increased Adiposity and Liver Hypertrophy

Deficiencies in TLR signaling by the intestinal epithelium have been associated previously with the development of MetS.^{19,20} Given that intestinal epithelial DUOX2 is essential in preventing microbial colonization of the mucosa,²⁴ we reasoned that insufficient DUOX2 activity may promote MetS. To test this hypothesis, we first asked whether DA IEC-KO mice with inactive intestinal DUOX2 developed obesity. DA IEC-KO mice and wild-type (WT) littermates of both sexes were placed on a standard chow diet (2018 Teklad Global Rodent Diet) and monitored for weight change from 10 to 24 weeks of age (Figure 1A). Weekly measurements of mouse body weight revealed a notable separation and increased trend in the body weights of male DA IEC-KO mice by 17 weeks, with a significant increase measured at 24 weeks, as compared with WT littermates (Figure 1B and C) (n = 5–10 per group; *P* = .022 at 24 weeks). Food consumption was

*Authors share co-first authorship; §Authors share co-senior authorship.

Abbreviations used in this paper: CEC, colonic epithelial cell; DA IEC-KO, dual oxidase A2 intestinal epithelial knockout; DUOX, dual oxidase; DUOXA, dual oxidase maturation factor; FD4, 4 kilodaltons fluorescein isothiocyanate-dextran; GTT, glucose tolerance test; IBD, inflammatory bowel disease; LPS, lipopolysaccharide; MetS, metabolic syndrome; MPO, myeloperoxidase; mRNA, messenger RNA; OCT, optimum cutting temperature; ORO, Oil-red-O; PBS, phosphate-buffered saline; ROS, reactive oxygen species; PV, portal vein; TLR, Toll-like receptor; sWAT, subcutaneous white adipose tissue; vLDL, very low density lipoprotein; WT, wild-type.

 Most current article

© 2023 The Authors. Published by Elsevier Inc. on behalf of the AGA Institute. This is an open access article under the CC BY-NC-ND license (<http://creativecommons.org/licenses/by-nc-nd/4.0/>).

2352-345X

<https://doi.org/10.1016/j.jcmgh.2023.06.009>

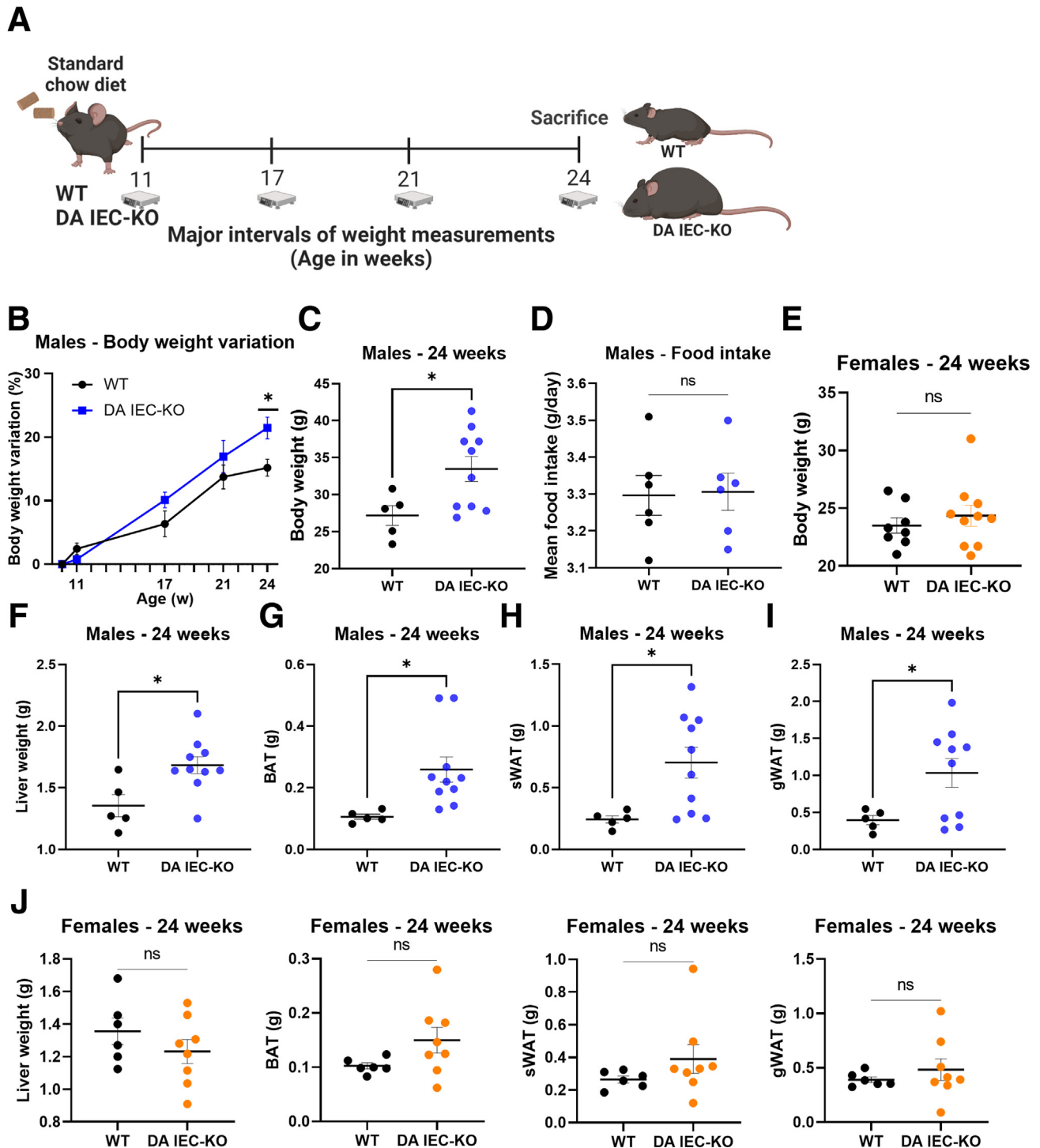


Figure 1. Intestinal epithelial inactivity of DUOX2 leads to increased adiposity and liver hypertrophy. (A) Schematic of experimental design: 10-week-old male DA IEC-KO and WT littermates underwent weekly body weight measurements until the age of 24 weeks. (B) Weekly body weight variation, in percentages, of DA IEC-KO and WT littermates (2-way analysis of variance). (C) Body weights of 24-week-old DA IEC-KO males ($n = 10$) and WT littermates ($n = 5$). (D) Mean measurements of food intake of DA IEC-KO mice and WT littermates ($n = 6$). (E) Body weights of 24-week-old DA IEC-KO females ($n = 10$) and WT littermates ($n = 8$). Twenty-four-week-old DA IEC-KO males ($n = 10$) and WT littermates ($n = 5$) of the same age were assessed for the following: (F) liver weight, (G) brown adipose tissue (BAT) weight, (H) sWAT weight, and (I) gonadal white adipose tissue (gWAT) weight. (J) Liver, BAT, sWAT, and gWAT weight measurements in 24-week-old DA IEC-KO females ($n = 10$) and WT littermates ($n = 8$). (C–J) Data were analyzed by unpaired t test. $*P < .05$.

similar between DA IEC-KO mice and WT littermates (Figure 1D) (n = 6 per group). Notably, female DA IEC-KO mice did not show any significant weight differences at 24 weeks of age (Figure 1E) (n = 8–10 per group).

To discern the effects of the observed body weight differences on organ and adipose tissue weights, 24-week-old DA IEC-KO males and their WT littermates were killed (Figure 1C) (n = 5–10; $P = .0308$) and internal organs were harvested. Compared with WT littermates (n = 5), DA IEC-KO mice (n = 10) had increased liver (Figure 1F) ($P = .0148$), brown adipose tissue (Figure 1G) ($P = .0020$), subcutaneous white adipose tissue (sWAT) (Figure 1H) ($P = .0244$), and gonadal white adipose tissue weights (Figure 1I) ($P = .0419$). Consistent with body weight data, liver and adipose tissue weights of female DA IEC-KO mice did not differ from WT littermates (Figure 1J) (n = 6–8 per group). Taken together, these results suggest that the loss of intestinal epithelial DUOX2 activity is sufficient to induce a marked sex-specific increase in body weight, adiposity, and liver weights at baseline conditions.

DA IEC-KO Mice Show Low-Grade Inflammation, Glucose Intolerance, and Lipid Accumulation in the Liver and Adipose Tissue

To determine if obesity in DA IEC-KO males is associated with a MetS phenotype, 24-week-old DA IEC-KO and WT littermates were subjected to a glucose tolerance test (GTT) before being killed, followed by blood, liver, and adipose tissue collection. Overall, GTT revealed impaired glucose tolerance in DA IEC-KO mice, with increased blood glucose levels at 0, 40, 60, 90, and 120 minutes after glucose oral gavage compared with WT littermates (Figure 2A) (n = 6–9; $P < .0001$). Other markers of MetS increased in DA IEC-KO mice, as compared with WT, included plasma triglycerides ($P = .0018$), total cholesterol ($P = .0283$), high-density lipoprotein ($P = .0153$), and very low-density lipoprotein (vLDL) ($P = .0010$) (Figure 2B) (n = 4–8 per group). In addition, plasma levels of the liver enzyme aspartate aminotransferase ($P = .0490$), alanine aminotransferase ($P = .0246$), and alkaline phosphatase ($P = .0131$), as well as the acute phase protein, serum amyloid A1 ($P = .0012$), were increased in DA IEC-KO males as compared with littermate controls (Figure 2C) (n = 4–7 per group), suggesting the development of low-grade inflammation. In contrast, no differences in blood glucose levels or other plasma analytes were observed in female DA IEC-KO mice compared with WT littermates (Figure 2D–F). Taken together, these findings uncover significant metabolic alterations in DA IEC-KO males.

Because adipocytes play key roles in regulating lipid and glucose metabolism,²⁸ we next analyzed distinct adipose tissues for lipid deposition and markers of metabolic dysfunction. Histologic assessment of brown adipose tissue revealed an increase in lipid droplet size per adipocyte in DA IEC-KO mice (Figure 3A) (n = 4–5; $P = .0011$), which is consistent with less thermogenic capabilities as observed in MetS.²⁹ Further supporting this notion, gene expression analysis revealed a marked down-regulation of the thermogenesis marker, uncoupling protein 1, in the sWAT of DA

IEC-KO mice (Figure 3B) (n = 5–8; $P < .0001$). Together, these results suggest an overall reduced thermogenic capacity of DA IEC-KO mice in adipose tissues that typically have thermogenic potential as shown in WT mice.³⁰ In addition, messenger RNA (mRNA) levels of the adipokine leptin (*Lep*) and the carbohydrate response element binding protein (*ChREBP*) were increased in the sWAT of DA IEC-KO males, whereas the mRNA transcript levels of adiponectin (*Adipoq*) were decreased, as compared with WT littermates (Figure 3B) (n = 5–8; $P < .001$). These results suggest that leptin, ChREBP, and *Adipoq* may be involved in DA IEC-KO-induced MetS.

To investigate whether intestinal epithelial DUOX2 inactivity promotes lipid accumulation and metabolic alterations in the liver, frozen sections were stained with Oil Red O dye (ORO). Livers of DA IEC-KO mice showed histopathologic features consistent with liver steatosis, including a significantly higher mean ORO score (Figure 3C) (DA IEC-KO, 2.8; vs WT, 0.3; n = 4–5; $P < .001$), indicating that 50%–75% of hepatocytes in these mice were occupied by lipids. Gene expression analysis on livers from DA IEC-KO mice revealed similar patterns of alterations as observed in sWAT, with an up-regulation of *Lep* and *ChREBP*, and a down-regulation of *Adipoq* (Figure 3D) ($P < .001$; n = 5). These data suggest that loss of DUOX2 signaling in the gut epithelium facilitates lipid accumulation and obesity.

To assess whether the observed changes in adipose tissue metabolism and lipid deposition were accompanied by inflammation or altered macrophage infiltration in our model, histologic and gene expression analyses were performed. Histologic analysis of H&E-stained slides revealed an increase in inflammatory foci in livers of DA IEC-KO males (Figure 3E) (n = 5; $P = .0022$). We also found that transcripts for the macrophage markers *Cd68* and *F4/80* (*Adgre1*) were up-regulated significantly in the sWAT and liver of DA IEC-KO mice as compared with WT littermates (Figure 3B and D) (n = 5–8; $P < .0001$ for both), indicating an increase in immune cell recruitment in these mice. This was confirmed further by immunofluorescence staining for *F4/80* in both sWAT (Figure 3F) (n = 4–5; $P < .001$) and liver (Figure 3G) (n = 4–5; $P < .001$). Overall, our findings show that the loss of DUOX2 activity in the intestinal epithelium provokes systemic biochemical, molecular, and tissue changes consistent with MetS.

Loss of Epithelial DUOX2 Activity Promotes Increased Gut Permeability and Bacterial Translocation to the Liver and Subcutaneous White Adipose Tissue

ROS play important roles in host antimicrobial defense.^{31,32} Indeed, loss-of-function mutations in DUOX2 are associated with increased pathogen invasiveness.^{24,33} To confirm that deletion of DUOX2 resulted in a lower production of ROS, we isolated colonic epithelial cells (CECs) and determined their expression of *Duox2* and *Duoxa2* as well as their release of extracellular hydrogen peroxide (Figure 4A). As expected, deletion of *Duoxa1/2* led to a significant down-regulation of *Duox2* transcripts, which functionally translated into a marked

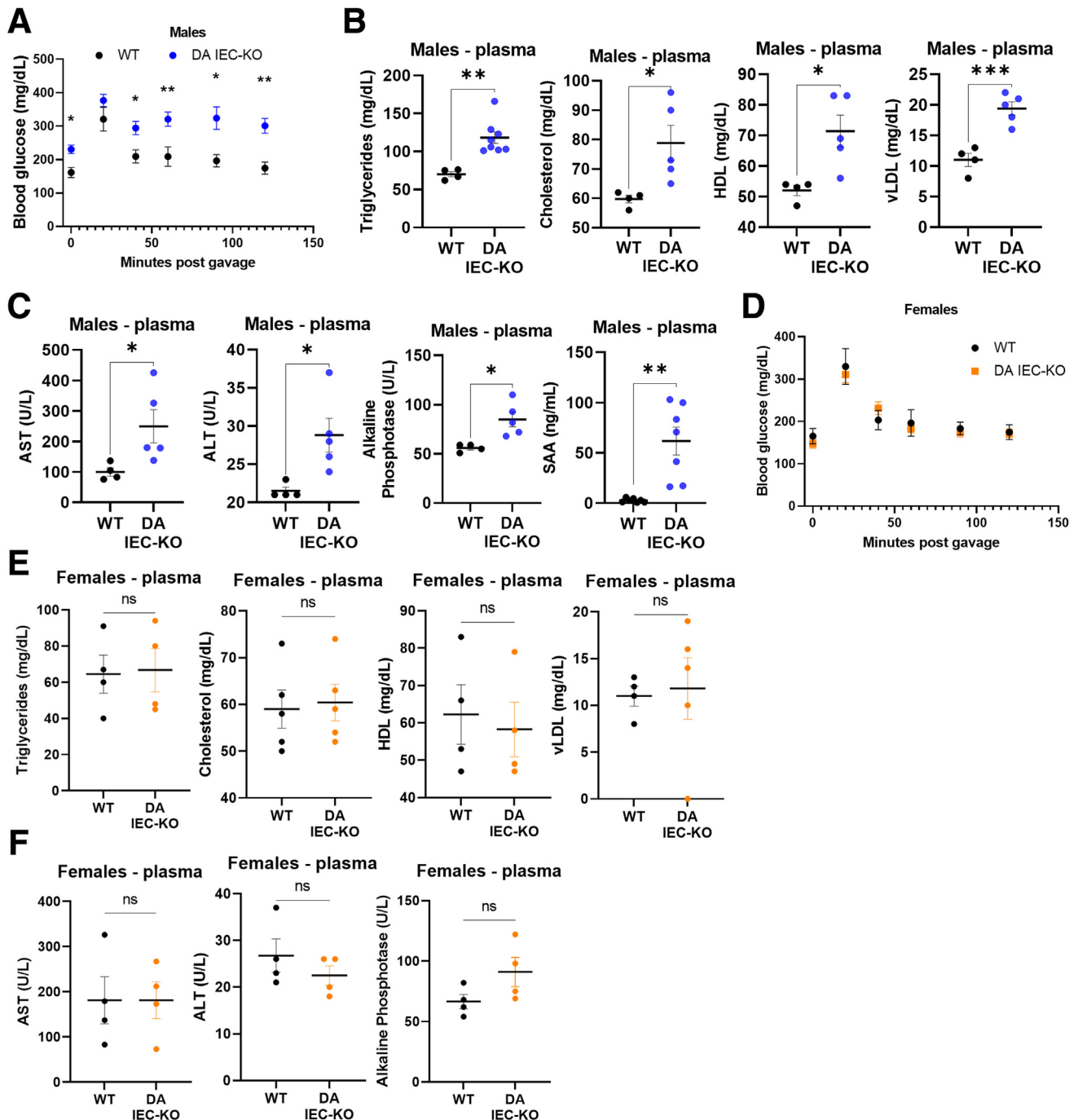


Figure 2. DA IEC-KO mice show low-grade inflammation and glucose intolerance. (A) Blood glucose levels in DA IEC-KO ($n = 9$) and WT ($n = 6$) littermates measured every 20–30 minutes after glucose gavage (2-way analysis of variance [ANOVA]). (B) Plasma triglyceride, total cholesterol, high density lipoprotein (HDL) and vLDL levels in DA IEC-KO ($n = 5$ –8) and WT ($n = 4$) littermates. (C) Plasma quantification of aspartate aminotransferase (AST), alanine aminotransferase (ALT), alkaline phosphatase, and serum amyloid A1 (SAA) in DA IEC-KO ($n = 5$) and WT ($n = 4$) littermates. (D) Blood glucose levels in female DA IEC-KO ($n = 10$) and WT ($n = 8$) mice (2-way ANOVA). (E) Quantification of triglyceride, total cholesterol, HDL and vLDL, and (F) AST, ALT, and alkaline phosphatase in plasma obtained from DA IEC-KO females and WT littermates ($n = 4$ for both groups). (B, C, E, and F) Data were analyzed by unpaired t test. $*P < .05$.

reduction in the production of H_2O_2 (Figure 4B and C) ($n = 4$ –8; $P < .0001$). Reduced H_2O_2 production also was observed in female DA IEC-KO mice (Figure 4D) ($n = 5$; $P < .001$). To determine whether loss of intestinal epithelial DUOX2 activity

modulates gut inflammation in 24-week-old mice, we examined H&E-stained colonic sections and probed colonic tissue for inflammatory gene expression and myeloperoxidase (MPO) activity. Histopathologic examination revealed that DA

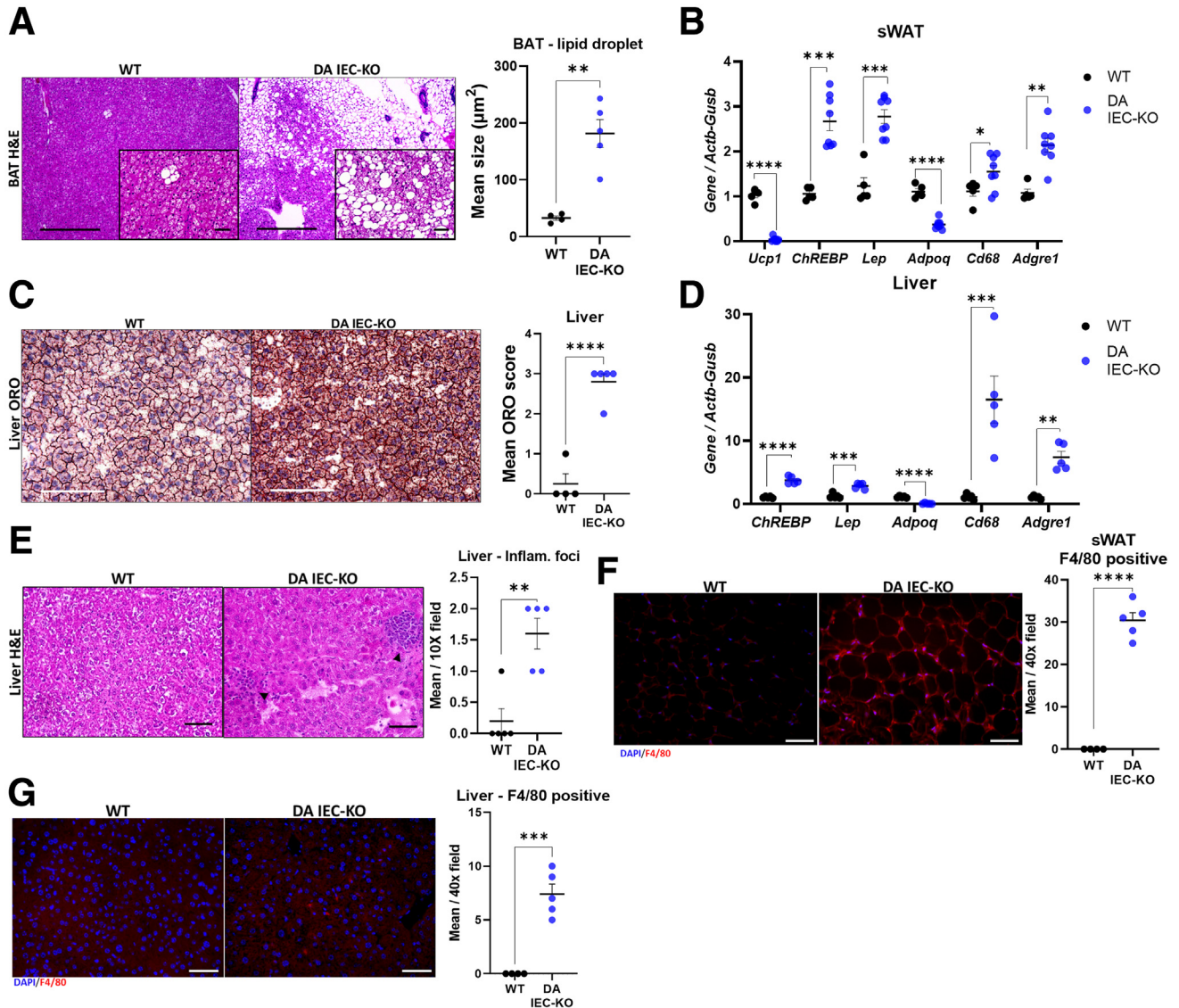


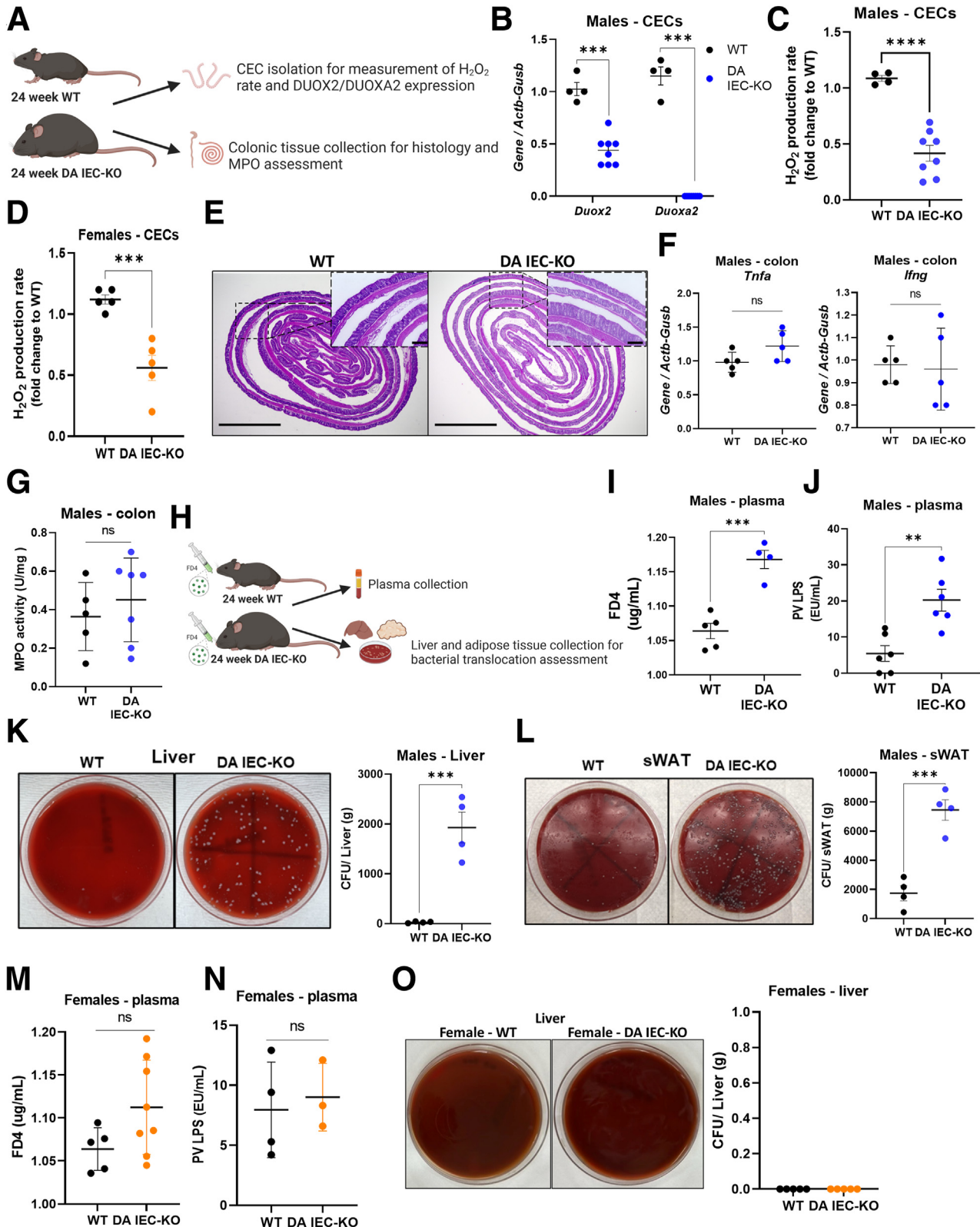
Figure 3. DA IEC-KO mice show lipid accumulation and macrophage infiltration in the liver and adipose tissue. (A) *Left:* Representative H&E images of brown adipose tissue (BAT) obtained from DA IEC-KO mice and WT littermates (scale bars: 200 μm ; inset scale bars: 25 μm). *Right:* Quantification of lipid droplet size from BAT images in DA IEC-KO mice ($n = 5$) and WT littermates ($n = 4$). (B) Gene expression quantification of *Ucp1*, *ChREBP*, leptin (*Lep*), *Adpoq*, *Cd68*, and *Adgre1* (*F4/80*) from sWAT obtained from DA IEC-KO ($n = 8$) and WT ($n = 5$) littermates. (C) *Left:* Representative images of livers stained with ORO and obtained from DA IEC-KO mice and WT littermates (scale bars: 200 μm). *Right:* Scoring of ORO stain calculated as a score from the percentage of tissue stained in DA IEC-KO mice compared with WT littermates ($n = 5$ for both groups) (ORO score: 0, 0%; 1, 1%–25%; 2, 26%–50%; 3, 51%–75%; and 4, 76%–100%). (D) Gene expression quantification of *ChREBP*, leptin (*Lep*), *Adpoq*, *Cd68*, and *Adgre1* (*F4/80*) from livers obtained from DA IEC-KO and WT littermates ($n = 5$ for both groups). (E) *Left:* Representative H&E microscopy images of liver tissue obtained from DA IEC-KO mice and WT littermates (scale bars: 25 μm). *Right:* Quantification of inflammatory foci from liver microscopy images in DA IEC-KO mice ($n = 5$) and WT littermates ($n = 5$). (F) *Left:* Representative F4/80 staining in sWAT tissue from DA IEC-KO and WT littermates (scale bars: 25 μm). *Right:* Quantification of F4/80-positive cells in sWAT ($n = 5$). (G) *Left:* Representative staining for F4/80 in liver tissue from DA IEC-KO and WT mice (scale bars: 25 μm). *Right:* Quantification of F4/80-positive cells ($n = 5$). (B–J) Data were analyzed by unpaired *t* test. * $P < .05$, ** $P < .01$, and *** $P < .001$. DAPI, 4',6-diamidino-2-phenylindole; Inflam, inflammation.

IEC-KO mice did not overtly differ from WT littermates in inflammation (Figure 4E). Furthermore, gene expression analysis revealed no significant differences in expression of the inflammatory cytokines *Tnfa* and *Ifng* between DA IEC-KO mice and WT littermates (Figure 4F) ($n = 5$). MPO activity, a

marker of neutrophil infiltration, also was not significantly different between the groups (Figure 4G) ($n = 5$ –7). Altogether, these data indicate that loss of DUOX2 signaling in the intestinal epithelium does not lead to overt colonic inflammation under homeostatic conditions.

Next, we sought to determine whether the reduction in DUOX2 activity led to alterations in epithelial barrier function, which have been linked to MetS. To that end, we

orally administered 4 kilodaltons of fluorescein isothiocyanate-dextran (FD4) to 24-week-old DA IEC-KO males and their WT littermates and collected blood to



determine the amount of fluorophore leaking from the gut into circulation (Figure 4H). We then collected PV blood and liver and adipose tissue to measure LPS levels and bacterial load in these tissues. Plasma FD4 levels were increased significantly in DA IEC-KO mice, indicating increased permeability in those mice (Figure 4I) ($n = 4-5$; $P = .0005$), as compared with WT littermates. This observation was supported further by increased LPS levels in the PV (Figure 4J) ($n = 6$; $P = .002$) and increased bacterial translocation to the liver (Figure 4K) ($n = 4$; $P < .0001$) and sWAT (Figure 4L) ($n = 4$; $P = .0006$) in DA IEC-KO mice. Interestingly, female DA IEC-KO mice did not have increased plasma levels of FD4 (Figure 4M) ($n = 5-8$), increased PV LPS levels (Figure 4N) ($n = 3-4$), or increased bacterial translocation to the liver (Figure 4O, $n = 5$), which may explain the lack of MetS phenotype in these mice. Overall, these data demonstrate that loss of DUOX2 activity in the gut does not lead to overt spontaneous intestinal inflammation but rather contributes to a leaky epithelial barrier that in turn facilitates bacterial translocation to distant sites in our model.

Loss of Intestinal Epithelial DUOX2 Activity Drives Functional and Compositional Alterations in the Gut Microbiome

To gain insight into the effect of reduced DUOX2 activity on the microbiome, we analyzed the composition of the fecal microbiota through shotgun metagenomic sequencing. Our results show that although loss of DUOX2 activity in our model did not shape α -diversity (Chao1 index) (Figure 5A) ($n = 5-7$), we observed a clear separation in a Bray-Curtis-based analysis of β -diversity between stool from DA IEC-KO males and WT littermates (Figure 5B) ($n = 5-7$). Overall, we observed that microbiota from DA IEC-KO mice clustered together in terms of relative abundance (Figure 5C and D) at both the phylum and family levels. In DA IEC-KO mice, we observed a marked expansion in the relative abundance of bacteria belonging to the family *Lachnospiraceae* (Figure 5D), which is implicated in several cardiometabolic diseases.^{34,35} Our data in DA IEC-KO mice also showed a striking reduction in relative abundance in bacteria from the family *Akkermansiaceae* (Figure 5D), which is associated with leanness and protection from obesity.³⁶ To gain insight into the functional state of the microbiota, we

performed pathway enrichment analysis. Many microbial pathways involved in amino acid (orange), carbohydrate and lipid (green), and energy (blue) metabolism were modulated significantly by DUOX2 activity (Figure 5E). Overall, our data indicate that changes in epithelial ROS production, specifically through DUOX2 deficiency, could alter the microbial community structure and function in the gut.

Antibiotic Depletion of the Microbiome Protects Against DUOX2-Deficiency-Mediated Mets

Increased bacterial translocation can cause chronic inflammation and MetS.²⁸ To test the involvement of the microbiome in the DUOX2-mediated metabolic alterations and underlying inflammation observed in our model, we first depleted the microbiome in DA IEC-KO and WT littermates by administering 1 g/L metronidazole and ciprofloxacin for 6 weeks (Figure 6A). After treatment with antibiotics, mice underwent a GTT before being killed. Body and organ weights were accounted for, and blood was collected. We found that antibiotic treatment completely abrogated the obesity and MetS phenotypes observed in DA IEC-KO males. Indeed, our results showed no difference in body or internal organ weights (Figure 6B-D) ($n = 5-11$) between antibiotic-treated DA IEC-KO and WT littermates. Consistent with these findings, we found no observable difference in blood glucose (Figure 6E) ($n = 5$), total cholesterol, high-density lipoprotein, vLDL, or triglyceride levels (Figure 6F) ($n = 5-11$) in the same comparison. Antibiotic treatment also ameliorated liver inflammation as measured by plasma aspartate aminotransferase, alanine aminotransferase, and alkaline phosphatase (Figure 6G) ($n = 4-5$). This was confirmed further by histology (Figure 6H). Importantly, antibiotic-treated DA IEC-KO mice still displayed altered permeability as measured by FD4 (Figure 6I) ($n = 4-5$). These data suggest that intestinal epithelial DUOX2 deficiency is enough to cause impaired barrier function, yet the microbiome is required for the low-grade inflammation and MetS phenotype observed in male mice.

Discussion

The intestinal epithelial barrier is the major interface between host and microbiota and as such could provide key mechanistic insights into the systemic influence of the microbiome on host health. Alterations in the gut microbiota

Figure 4. (See previous page). Loss of epithelial DUOX2 activity promotes increased gut permeability and bacterial translocation to the liver and sWAT. (A) Schematic of experiments performed for data presented in panels B–G. (B) *Duox2* and *Duoxa2* gene expression analysis of mRNA extracted from freshly isolated CECs obtained from DA IEC-KO mice ($n = 8$) and WT littermates ($n = 4$). Quantification of H₂O₂ production rates from freshly isolated CECs obtained from (C) male DA IEC-KO ($n = 8$) and (D) female DA IEC-KO ($n = 5$) and WT ($n = 4-5$) littermates. (E) Representative H&E images of colon sections from DA IEC-KO males and WT littermates (scale bars: 200 μ m; inset scale bars: 25 μ m). (F) *Tnfa* and *lfn3* gene expression analysis on mRNA extracted from whole colons obtained from DA IEC-KO males and WT littermates ($n = 5$). (G) Quantification of MPO activity from colonic tissue obtained from DA IEC-KO ($n = 7$) and WT ($n = 5$) littermates. (H) Schematic of experiments for data presented in panels I–O. Quantification of plasma (I) FD4 and (J) PV LPS from male DA IEC-KO ($n = 4$) and WT ($n = 4-5$) littermates. Left: Representative macroscopic images of (K) bacterial cultures cultivated from liver and (L) sWAT homogenates obtained from male DA IEC-KO mice and WT littermates. Right: Quantification of (K) colony forming units (CFU) per gram of liver and (L) sWAT tissue ($n = 4$). Quantification of plasma (M) FD4 and (N) PV LPS obtained from DA IEC-KO females ($n = 4-8$) and WT littermates ($n = 4-5$). Left: Representative macroscopic images of bacterial cultures cultivated from liver homogenates obtained from female DA IEC-KO mice and WT littermates. Right: Quantification of colony forming units per gram of liver tissue ($n = 5$). Data were analyzed by unpaired *t* test. ** $P < .01$, *** $P < .001$, **** $P < .0001$.

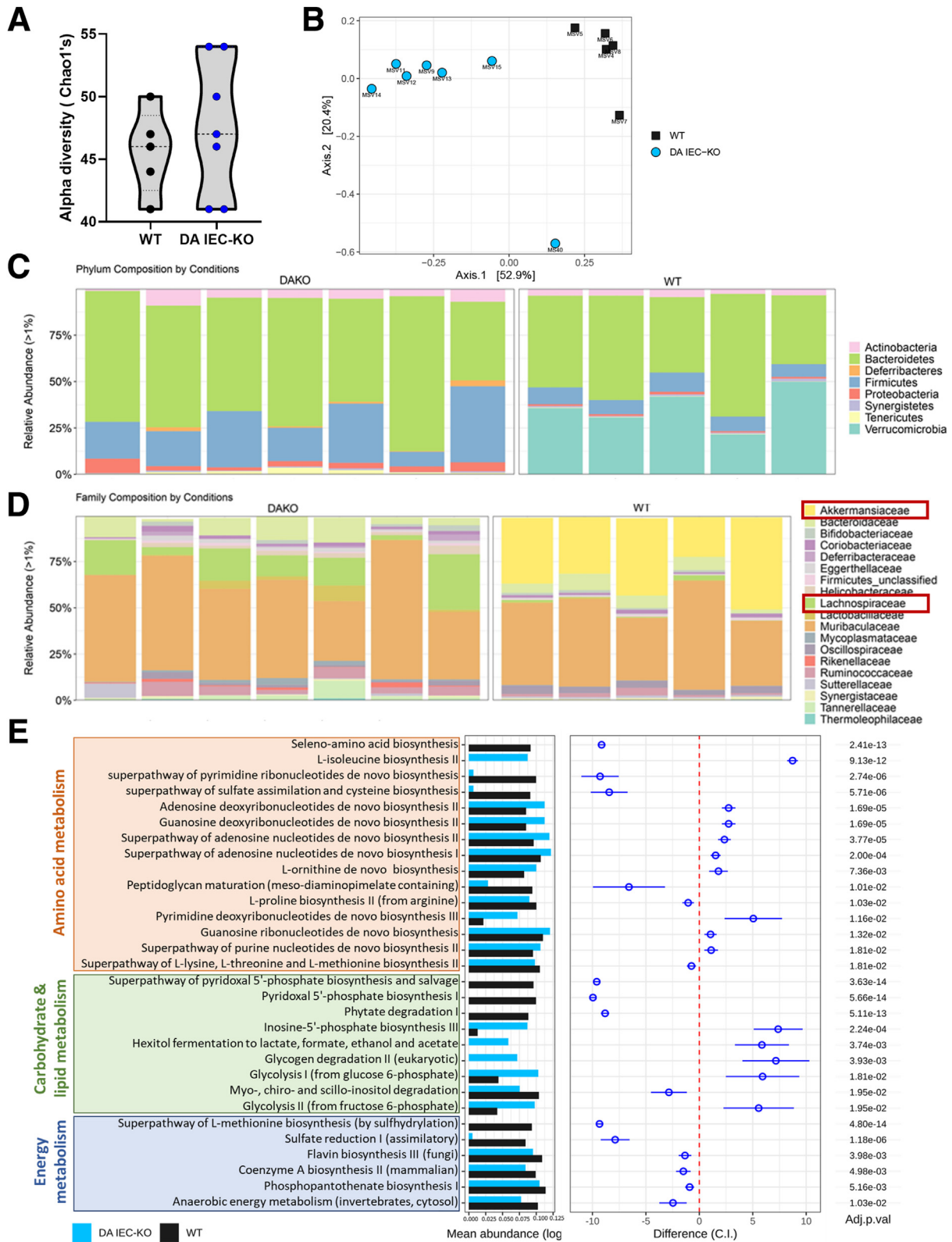
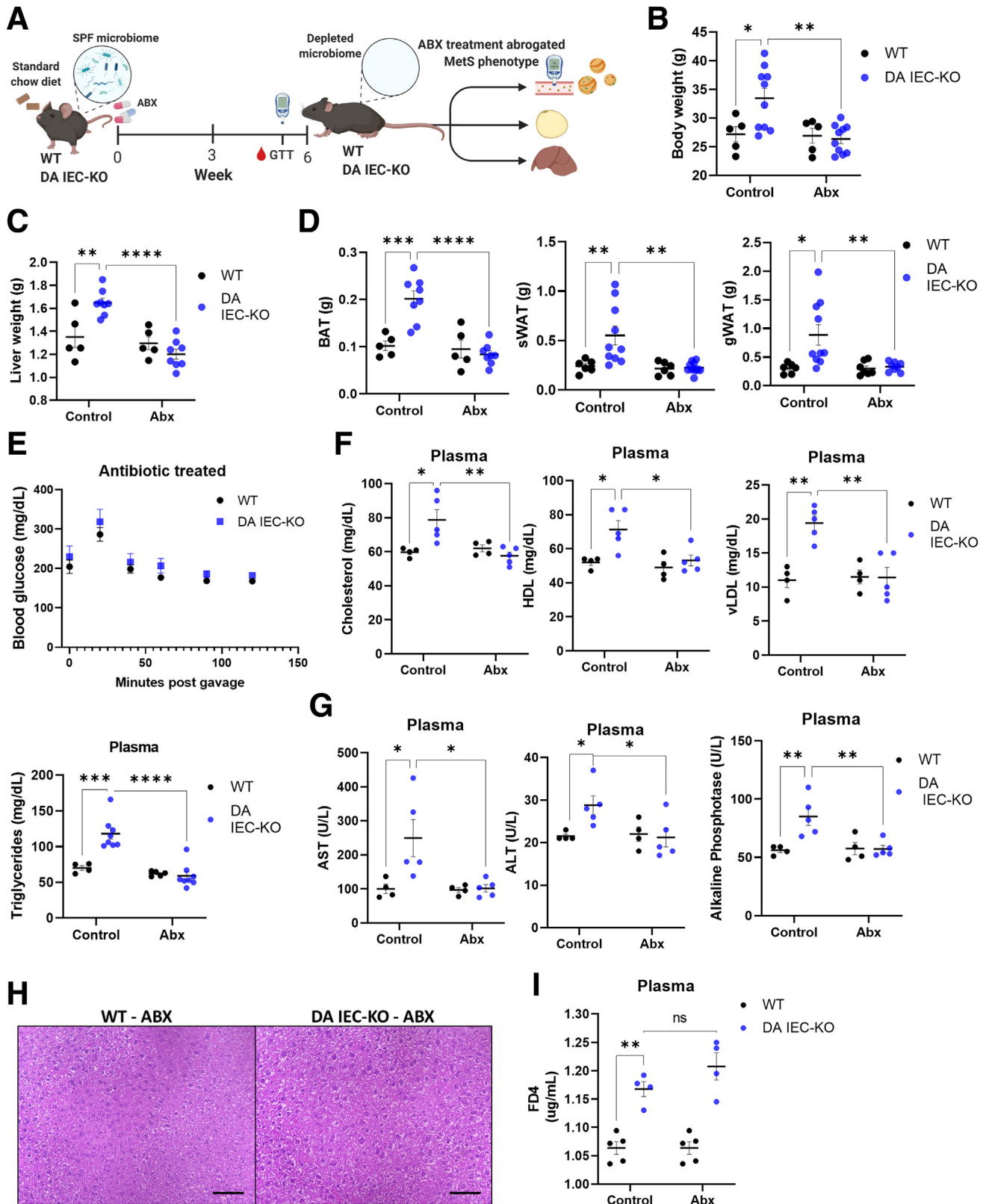


Figure 5. Loss of intestinal epithelial DUOX2 drives functional and compositional alterations in the gut microbiome. (A) α -diversity (Chao1's) analysis on metagenomic sequencing data of stool obtained from DA IEC-KO mice (n = 7) and WT littermates (n = 5). (B) Principal coordinate analysis based on Bray–Curtis dissimilarity on metagenomic sequencing data of stool obtained from DA IEC-KO mice (n = 7) and WT littermates (n = 5). Relative abundance of taxa identified in stool obtained from DA IEC-KO mice (n = 7) and WT littermates (n = 5) on the (C) phylum and (D) family taxonomic rank level. (E) Pathway analysis on metagenomic sequencing data of stool obtained from DA IEC-KO mice (n = 7) and WT littermates (n = 5) highlighting pathways involved in amino acid (orange), carbohydrate and lipid (green), and energy metabolism (blue).

are linked not only to the development of local gut pathologies, such as IBD, but are critical in systemic disorders such as obesity, dyslipidemia, hyperglycemia, and MetS.^{37,38} Here,

we add to the body of evidence showing that events occurring in the gut epithelium orchestrate systemic, microbiome-dependent consequences. Specifically, we demonstrate a



direct mechanistic link between the loss of epithelial-specific DUOX2 activity and the development of MetS.

DUOX2 plays an essential role in mediating the interaction between the intestinal epithelium and the microbiota^{21,22} and is expressed at the tips of the intestinal crypts, where interaction with the microbiota occurs.²¹ In the current study, we show a novel role of intestinal epithelial DUOX2 in protecting against the development of MetS. Specifically, we show that deletion of epithelial DUOX2 leads to a reduction in H₂O₂ levels and a shift in microbial community structure that is reminiscent of what is seen in MetS. Our analysis showed a striking imbalance of 2 bacterial families in the stool of DA IEC-KO mice: *Akkermansia* and *Lachnospiraceae*. *Akkermansia*, which are reduced in DA IEC-KO mice, are present in the gut microbiome predominantly as *A muciniphila*. Although the effects of *A muciniphila* differ by model, it has stood out recently for its protective effect in obesity and metabolic disorders,^{39–42} possibly through increasing thermogenesis and regulating glucose and carbohydrate metabolism.⁴³ Conversely, *Lachnospiraceae*, which are enriched in our DA IEC-KO animals, are shown to impair glucose metabolism⁴⁴ and are increased in patients with nonalcoholic fatty liver disease.⁴⁵ Our data show that even in littermate controls, inactivation of epithelial DUOX2 was sufficient to shape the microbiome in an obesogenic fashion. Although microbiome modulation therapy, such as fecal microbiota transplantation, has shown some success, a challenge remains in preventing the microbiome from reverting to its dysbiotic state over time.^{46,47} Our studies support a role for improving epithelial barrier function in the treatment of MetS alongside microbial manipulation.⁴⁸

Several studies have indicated that both genetic and diet-induced models of obesity and MetS are characterized by an increase in gut permeability,^{49,50} however, the mechanisms by which this occurs remained to be elucidated. Here, we report that the absence of DUOX2 signaling increases gut permeability and permits bacterial translocation to target organs including the liver and adipose tissue depots. Our findings show a nonredundant role of DUOX2 in preserving epithelial barrier function and align with reports linking global DUOX2 deficiency and increased bacterial invasion of the mucosa.²⁴ In a separate report, one group described no overt epithelial barrier defects in 12-week-old global knockouts of DUOX2.²² The global DUOX2 KO animals used were on continuous hormone replacement therapy for hypothyroidism and differed from ours in age and genetic

background.²² Furthermore, it was unclear whether the investigators of the study used mice of both sexes.

Our study examined various dimensions of MetS at the level of adipose tissue regulation and its effect on glucose and lipid metabolism. We show that the leaky epithelial barrier caused by DUOX2 deficiency leads to bacterial translocation, which in turn induces adipose tissue inflammation and leads to impaired adipose tissue thermogenesis, adipokine dysregulation, lipid accumulation, and glucose intolerance. DA IEC-KO mice had high leptin and low adiponectin levels in the liver and adipose tissue consistent with obesity⁵¹ and leptin resistance.^{52,53} These mice also had up-regulated expression of the glucose-sensing molecule ChREBP, its increase was associated with steatosis through promoting de novo lipogenesis and triglyceride and vLDL accumulation.⁵⁴ Altogether, our data suggest that intestinal epithelial DUOX2 plays a role in MetS by influencing lipid and glucose metabolism.

Sex differences in MetS are important to characterize if we are to be successful in developing interventions. We observed a striking absence of MetS in female mice. This finding is consistent with reports describing that male mice are more vulnerable to glucose and metabolic disturbances than females and thus are used more frequently in metabolic and obesity studies.^{55–57} Interestingly, female DA IEC-KO mice displayed a trend of increased serum FD4 level after oral gavage that did not reach significance and had no increased PV LPS levels or bacterial translocation to the liver (Figure 4M–O), unlike their male counterparts. This lack of overt permeability defects may account for the resistance of females to the development of MetS in our model. Why female mice are protected from the DUOX2-dependent barrier dysfunction requires further study, including analyzing the microbiome for its potential impact on epithelial barrier integrity.⁵⁸

Overall, our current study shows that DUOX2 enzymatic deficiency in the intestinal epithelium of mice leads to MetS in a microbiome-dependent manner. Microbiome depletion, through antibiotic treatment, reversed the MetS phenotype. These data confirm that the mechanism by which DUOX2 protects against the development of MetS is through epithelial barrier protection and limiting bacterial translocation. As such, our current findings elucidate a novel mechanism and target for the treatment of MetS, but also as a potential target for other diseases that are marked by gut epithelial barrier alterations. Our data point to additional

Figure 6. (See previous page). Antibiotic depletion of the microbiome protects against DUOX2-deficiency-mediated MetS. (A) Schematic of experimental design. DA IEC-KO and WT littermates underwent microbiome depletion through antibiotic administration. Twenty-four-week-old microbiome-depleted DA IEC-KO mice (n = 6) and WT littermates (n = 5) of the same age were assessed for: (B) body weight, (C) liver weight, (D) brown adipose tissue (BAT) weight, sWAT weight, and gonadal white adipose tissue (gWAT) weight. (E) Microbiome-depleted DA IEC-KO mice and WT littermates (n = 6 for both groups) underwent a glucose tolerance test and blood glucose levels were measured every 20–30 minutes, after glucose gavage (2-way analysis of variance [ANOVA]). (F) Plasma total cholesterol, high-density lipoprotein (HDL), vLDL, and triglyceride, (G) aspartate aminotransferase (AST), alanine aminotransferase (ALT), and alkaline phosphatase quantification of microbiome-depleted DA IEC-KO (n = 6–8) mice compared with WT (n = 4–5) mice. (H) Representative microscopy images of liver tissue stained with H&E obtained from DA IEC-KO mice compared with WT mice (scale bars: 25 μm), n = 4 for both. (I) Quantification of FD4 present in plasma obtained from microbiome-depleted DA IEC-KO (n = 4) and WT (n = 5) mice after oral administration. Data were analyzed by 2-way ANOVA. *P < .05, **P < .01, ***P < .001, and ****P < .0001. Abx, antibiotics; SPF, specific pathogen free.

potential points of intervention in the prevention or treatment of MetS.

Conclusions

In conclusion, our results show that defective epithelial-specific host antimicrobial defenses promote metabolic syndrome, and that the microbiota is necessary for this pathology.

Materials and Methods

Animals

DA IEC-KO mice, which bear functionally deficient DUOX1 and DUOX2 in the gut epithelium, were obtained by crossing the *Duoxa1/2*-floxed mice (generated at the Mouse Biology Program at University of California Davis under the auspices of Dr Kaunitz's laboratory [University of California Los Angeles]) with villin-cre (Tg[Vil1-cre]997Gum) mice purchased from Jackson Laboratory. These mice are widely accepted as a model to investigate the role of intestinal DUOX2 because the expression of DUOX1 in the gut is exceedingly low.²² These mice, generated on a C57Bl/6 background, and their WT littermates (*Duox1/2*-floxed, villin-cre negative), were sexed, separated, randomized, and housed in specific pathogen-free conditions with a controlled temperature of 20°C ± 2°C. Mice were fed the 2018 Teklad Global 18% Protein Rodent Diet under free access to food and water. Follow-up evaluation of mouse body weight started at 10 weeks of age and terminated at 24 weeks. Food intake was measured manually twice a day for 2 weeks. To deplete the microbiome, 18-week-old mice were placed on the broad-spectrum antibiotics metronidazole and ciprofloxacin (1.0 g/L each) in drinking water for 6 weeks as previously described.⁵⁹ Most procedures were performed between 18 and 24 weeks of age with the approval of the Institutional Animal Care and Use Committee at the University of Miami and the VA Greater Los Angeles Healthcare System (protocol number 1616031-3). The University of Miami and the West Los Angeles VAMC are internationally accredited by the Association for Assessment and Accreditation of Laboratory Animal Care.

Glucose Tolerance Test and Triglyceride Determination

Mice (age, 24 wk) were placed in clean cages and fasted for 6 hours before oral administration of 2 g glucose/kg mouse body weight (Sigma-Aldrich). Blood was sampled from the tail every 20–30 minutes for 2 hours after injection and blood glucose was measured at each time point using a glucometer (Clarity Diagnostics). Circulating triglyceride levels were measured through an enzymatic colorimetric assay on plasma collected from 24-week-old mice, and values were calculated through the use of a standard curve.

Fluorescein Isothiocyanate–Dextran Permeability Assessment

The 24-week-old mice underwent food restriction for 12 hours before receiving a 600-mg/kg oral gavage of 4 kilodaltons fluorescein isothiocyanate–dextran. Four hours later, blood was

collected and fluorescein isothiocyanate fluorescence (485/528 nm ex/em) in separated plasma was read in a Synergy H1 fluorometer (BioTek). All samples were assayed in triplicate.

Euthanasia and Sample Collection

Mice were killed by cervical dislocation under isoflurane (Piramal Critical Care) anesthesia before blood collection by cardiac puncture. Fifteen milliliters phosphate-buffered saline (PBS) subsequently was injected in the left ventricle of the heart. Perfused organs including the liver, colon, and adipose tissue were harvested. After removing the gut from the peritoneal cavity, stool was flushed and collected, and the colon was used for isolation of CECs for measurement of H₂O₂ production and for RNA extraction. Liver and adipose tissue were weighed, sectioned, and either homogenized in TRIzol reagent (Thermo-Fisher Scientific) for RNA isolation, homogenized in PBS (Lonza) for microbiology plating, fixed in 4% paraformaldehyde for histology, or embedded in optimum cutting temperature (OCT) to prepare frozen tissue sections.

Bacterial Translocation Assessment

Homogenized livers and sWATs were cultured on tryptic soy sheep blood agar plates (Lonza) and incubated under aerobic and anaerobic conditions for 24 to 48 hours. Colonization was expressed as the average number of colony-forming units per milligram of tissue.

PV LPS Concentration Measurement

PV blood was collected from WT and DA IEC-KO mice under propofol anesthesia after 2 hours of fasting (to avoid any influence of diet and coprophagy) at age 20–24 weeks into a tube containing 1 μL of 0.5 mol/L EDTA. Samples were centrifuged at 5000 × *g* for 10 minutes and plasma was kept at -80°C until analysis. LPS levels in the PV plasma were measured by a limulus amoebocyte lysate test (Pierce Chromogenic Endotoxin Quant Kit; Pierce Biotechnology, Rockford, IL) as previously reported.⁶⁰

Isolation of Colonic Epithelial Cells and Measurement of Epithelial H₂O₂ Production

CECs were isolated by chelation, as previously described.²³ In brief, CECs were incubated in 20 mmol/L EDTA in Hank's balanced salt solution for 1 hour in a shaker at room temperature, followed by gentle shaking to release the crypts. Released crypts then were either lysed in TRIzol reagent for quantitative polymerase chain reaction or pelleted for determination of H₂O₂ production by a modified Amplex Red assay (Biotium). For H₂O₂ determinations, CECs were seeded in a 96-well plate and incubated in Dulbecco's PBS solution containing Ca²⁺, Mg²⁺, 10 mmol/L phenylmethylsulfonyl fluoride, 0.1 U/mL horseradish peroxidase, and 30 μmol/L Amplex red. Fluorescence was read at 40- to 60-second intervals for 10 minutes at 37°C (530/590 nm ex/em) in a Synergy H1 fluorometer. H₂O₂ production was normalized to cell viability via MTT ((3-(4,5-Dimethylthiazol-2-yl)-2,5-Diphenyltetrazolium Bromide)) assay

(American Type Culture Collection) as per the manufacturer's instructions. All samples were assayed in triplicate.

MPO Activity

Snap-frozen colon sections were homogenized in 50 mmol/L phosphate buffer containing 13.7 mmol/L hexadecyltrimethylammonium bromide (Sigma Aldrich) by means of a bead mill homogenizer (OMNI International). MPO activity of the supernatants was determined by measuring their ability to oxidize o-dianisidine (Sigma Aldrich) in the presence of H₂O₂ and interpolating their values to those of a known MPO standard. The MPO activity was normalized to the initial weight of each sample.

Histologic Evaluation

For ORO staining, mouse livers were embedded in OCT and stored at -80°C. Sections (12 μm) were cut from frozen OCT blocks and mounted to microscope slides. Freshly sectioned tissue slides were stained in filtered ORO for 15 minutes, followed by 2 wash steps in water for 5 minutes each. Tissue sections then were stained with hematoxylin for 2 minutes, after which coverslips were mounted with glycerol and allowed to air-dry overnight. For quantification, micrographs were taken at 10× or 40× magnification in a BZ-X700 microscope (Keyence). For scoring of lipid accumulation, images were given a score depending on the level of stain observed as follows: 0, no ORO stain; 1, 1%–25%; 2, 25%–50%; 3, 50%–

75%; and 4, 75%–100%. To account for lipid droplet size, area measurements were performed using ImageJ software (National Institutes of Health). For immunofluorescence, deparaffinized tissues mounted in slides underwent the initial antigen retrieval step by boiling in citric acid for 30 minutes. Unspecific binding was blocked by incubating tissue sections for 1 hour in PBS containing 0.5% Tween-20 and 5% goat serum. Tissue sections were treated overnight at 4°C with primary antibodies (rat anti-mouse F4/80 antibody, clone A3-1, MCA497GA, Bio-Rad) diluted in 5% goat serum solution. Next, tissue sections were incubated with secondary antibodies and counterstained with 4',6-diamidino-2-phenylindole (D9542, 500 nmol/L; Millipore Sigma). All slides were imaged under a BZ-X700 microscope (Keyence).

Quantitative Polymerase Chain Reaction Analysis

RNA from CECs, liver, or sWAT tissue was isolated using the phenol–chloroform extraction method.⁶¹ A total of 500 ng RNA was used for reverse-transcription via the PrimeScript RT reagent Kit (Takara Bio, Inc). The resulting complementary DNA then was amplified on a Light-Cycler 480 II instrument (Roche Applied Science) using SYBR Premix Ex Taq (Takara). A list of the primers used is provided in Table 1. mRNA expression levels were calculated using the ΔΔCt method,⁶² and normalized to the geometric mean of the housekeeping genes β-actin and/or glucuronidase-β.

Table 1. Quantitative Polymerase Chain Reaction Primers

Gene	Sense	Primer	Reference
<i>Actb</i>	Forward	TGACAGGATGCAGAAGGAGA	63
	Reverse	CGCTCAGGAGGAGCAATG	
<i>Duox2</i>	Forward	TCCAGAAGGCGCTGAACAG	NM_001362755.1
	Reverse	GCGACCAAAGTGGGTGATG	
<i>Duoxa2</i>	Forward	GCCTGGCTTTGCTCACCA	22
	Reverse	GAGGAGGAGGCTCAGGAT	
<i>Gusb</i>	Forward	CCGATTATCCAGAGCGAGTATG	64
	Reverse	CTCAGCGGTGACTGGTTCCG	
Epsilonproteobacteria	Forward	TAGGCTTGACATTGATAGAATC	65
	Reverse	CTTACGAAGGCAGTCTCCTTA	
Bacteroidetes	Forward	GTTTAATTCGATGATACGCGAG	65
	Reverse	TTAASCCGACACCTCACGG	
Eubacteria	Forward	AGAGTTTGATCCTGGCTCAG	66
	Reverse	AAGGAGGTGWTCCARCC	
<i>Ucp1</i>	Forward	AGGCTTCCAGTACCATTAGGT	67
	Reverse	CTGAGTGAGGCAAAGCTGATTT	
<i>Cd68</i>	Forward	TGTCTGATCTTGCTAGGACCG	68
	Reverse	GAGAGTAACGGCCTTTTTGTGA	
<i>Adgre1</i> (F4/80)	Forward	TGACTCACCTTGTTGGTCTTAA	69
	Reverse	CTTCCCAGAATCCAGTCTTTCC	
Adipoq	Forward	TCATTATGACGGCAGCAC	51
	Reverse	CCAGATGGAGGAGCACAG	
<i>ChREBP</i>	Forward	AGGCTTCCAGTACCATTAGGT	51
	Reverse	CTGAGTGAGGCAAAGCTGATTT	
Leptin	Forward	TGTCTGATCTTGCTAGGACCG	51
	Reverse	GAGAGTAACGGCCTTTTTGTGA	

DNA Extraction and Metagenomic Sequencing

Prokaryotic DNA was isolated from stool using the PowerSoil/fecal DNA Isolation Kit (MoBio Laboratories). DNA samples were submitted to the Sylvester Oncogenomics Shared Resources for microbiome shotgun sequencing. A buffer exchange, using 1× Ampure Beads (A63881; Beckman Coulter), was performed on the sample to remove contaminants before library preparation, using Kapa HyperPlus kits (Roche). Sequencing was performed on an Illumina NovaSeq 6000 using SBS chemistry in pair-end mode with 101 cycles for each end. Shotgun sequence reads were trimmed and filtered, and host DNA contaminated reads were removed using KneadData workflow (<https://huttenhower.sph.harvard.edu/kneaddata>). Metagenomic profiling of microbial abundance and taxonomy assignment was performed with MetaPhlan (ver.2),⁷⁰ which uses clade-specific marker genes from 17,000 reference genomes. Functional composition was determined using HUMAnN2⁷¹ with the complete UniProt Reference Clusters (UniRef) gene family,⁷² Kyoto Encyclopedia of Genes and Genomes (KEGG) functional modules and pathways,⁷³ and MetaCyc metabolic pathway databases.⁷⁴ α -diversity was calculated as Chao1 index, multidimensional scaling analysis plots of β -diversity were calculated based on Bray–Curtis distance, and the association of DA IEC-KO condition and β -diversity was analyzed based on the permutational analysis of variance test using methods provided by the phyloseq⁷⁵ and vegan⁷⁶ Bioconductor packages. Differential relative abundance of individual taxa, gene families, KEGG modules and pathways, and metabolic pathways was performed using a linear model for centered-log-ratio transformed abundance. The differential microbial features were selected based on multiple-hypothesis adjusted *P* value (False Discovery Rate, FDR) < .05.

Bioinformatics and Statistical Analysis

Results are presented as means \pm SEM. Data analysis and plots were performed using Prism8 (GraphPad Software, Inc) and compared using an unpaired Student *t* test and 2-way analysis of variance, as indicated. A *P* value less than .05 was considered significant.

References

- Miranda PJ, DeFronzo RA, Califf RM, Guyton JR. Metabolic syndrome: definition, pathophysiology, and mechanisms. *Am Heart J* 2005;149:33–45.
- Saklayen MG. The global epidemic of the metabolic syndrome. *Curr Hypertens Rep* 2018;20:12.
- Hill JO. Understanding and addressing the epidemic of obesity: an energy balance perspective. *Endocr Rev* 2006;27:750–761.
- Hales CM, Carroll MD, Fryar CD, Ogden CL. Prevalence of obesity among adults and youth: United States, 2015–2016. *NCHS Data Brief* 2017;288:1–8.
- Warnberg J, Marcos A. Low-grade inflammation and the metabolic syndrome in children and adolescents. *Curr Opin Lipidol* 2008;19:11–15.
- El Aidy S, Derrien M, Aardema R, et al. Transient inflammatory-like state and microbial dysbiosis are pivotal in establishment of mucosal homeostasis during colonization of germ-free mice. *Benef Microbes* 2014;5:67–77.
- Gomez-Hurtado I, Santacruz A, Peiro G, et al. Gut microbiota dysbiosis is associated with inflammation and bacterial translocation in mice with CCl₄-induced fibrosis. *PLoS One* 2011;6:e23037.
- Brandl K, Schnabl B. Is intestinal inflammation linking dysbiosis to gut barrier dysfunction during liver disease? *Expert Rev Gastroenterol Hepatol* 2015;9:1069–1076.
- Turnbaugh PJ, Backhed F, Fulton L, Gordon JI. Diet-induced obesity is linked to marked but reversible alterations in the mouse distal gut microbiome. *Cell Host Microbe* 2008;3:213–223.
- Drissi F, Raoult D, Merhej V. Metabolic role of lactobacilli in weight modification in humans and animals. *Microb Pathog* 2017;106:182–194.
- Lau K, Srivatsav V, Rizwan A, et al. Bridging the gap between gut microbial dysbiosis and cardiovascular diseases. *Nutrients* 2017;9:859.
- Backhed F, Manchester JK, Semenkovich CF, Gordon JI. Mechanisms underlying the resistance to diet-induced obesity in germ-free mice. *Proc Natl Acad Sci U S A* 2007;104:979–984.
- Backhed F, Ding H, Wang T, et al. The gut microbiota as an environmental factor that regulates fat storage. *Proc Natl Acad Sci U S A* 2004;101:15718–15723.
- Turnbaugh PJ, Ley RE, Mahowald MA, et al. An obesity-associated gut microbiome with increased capacity for energy harvest. *Nature* 2006;444:1027–1031.
- Ridaura VK, Faith JJ, Rey FE, et al. Gut microbiota from twins discordant for obesity modulate metabolism in mice. *Science* 2013;341:1241214.
- Hand TW, Vujkovic-Cvijin I, Ridaura VK, Belkaid Y. Linking the microbiota, chronic disease, and the immune system. *Trends Endocrinol Metab* 2016;27:831–843.
- Depommier C, Everard A, Druart C, et al. Supplementation with *Akkermansia muciniphila* in overweight and obese human volunteers: a proof-of-concept exploratory study. *Nat Med* 2019;25:1096–1103.
- Burgueno JF, Abreu MT. Epithelial Toll-like receptors and their role in gut homeostasis and disease. *Nat Rev Gastroenterol Hepatol* 2020;17:263–278.
- Lu P, Sodhi CP, Yamaguchi Y, et al. Intestinal epithelial Toll-like receptor 4 prevents metabolic syndrome by regulating interactions between microbes and intestinal epithelial cells in mice. *Mucosal Immunol* 2018;11:727–740.
- Chassaing B, Ley RE, Gewirtz AT. Intestinal epithelial cell toll-like receptor 5 regulates the intestinal microbiota to prevent low-grade inflammation and metabolic syndrome in mice. *Gastroenterology* 2014;147:1363–1377 e1317.
- Burgueno JF, Fritsch J, González EE, et al. Epithelial TLR4 signaling activates DUOX2 to induce microbiota-driven tumorigenesis. *Gastroenterology* 2021;160:797–808 e796.
- Grasberger H, Gao J, Nagao-Kitamoto H, et al. Increased expression of DUOX2 is an epithelial response to mucosal dysbiosis required for immune homeostasis in mouse intestine. *Gastroenterology* 2015;149:1849–1859.

23. Burgueno JF, Fritsch J, Santander AM, et al. Intestinal epithelial cells respond to chronic inflammation and dysbiosis by synthesizing H₂O₂. *Front Physiol* 2019;10:1484.
24. Hayes P, et al. Defects in NADPH oxidase genes NOX1 and DUOX2 in very early onset inflammatory bowel disease. *Cell Mol Gastroenterol Hepatol* 2015;1:489–502.
25. Levine AP, Pontikos N, Schiff ER, et al. Genetic complexity of Crohn's disease in two large Ashkenazi Jewish families. *Gastroenterology* 2016;151:698–709.
26. Grasberger H, Magis AT, Sheng E, et al. DUOX2 variants associate with preclinical disturbances in microbiota-immune homeostasis and increased inflammatory bowel disease risk. *J Clin Invest* 2021;131:e141676.
27. Parlato M, Charbit-Henrion F, Hayes P, et al. First identification of biallelic inherited DUOX2 inactivating mutations as a cause of very early onset inflammatory bowel disease. *Gastroenterology* 2017;153:609–611 e603.
28. Cani PD, Osto M, Geurts L, Everard A. Involvement of gut microbiota in the development of low-grade inflammation and type 2 diabetes associated with obesity. *Gut Microbes* 2012;3:279–288.
29. Gomez-Hernandez A, Beneit N, Diaz-Castroverde S, Escribano O. Differential role of adipose tissues in obesity and related metabolic and vascular complications. *Int J Endocrinol* 2016;2016:1216783.
30. Kontani Y, Wang Y, Kimura K, et al. UCP1 deficiency increases susceptibility to diet-induced obesity with age. *Aging Cell* 2005;4:147–155.
31. Alvarez LA, Kovačić L, Rodríguez J, et al. NADPH oxidase-derived H₂O₂ subverts pathogen signaling by oxidative phosphorylation conversion to PB-DOPA. *Proc Natl Acad Sci U S A* 2016;113:10406–10411.
32. Corcionivoschi N, Alvarez LAJ, Sharp TH, et al. Mucosal reactive oxygen species decrease virulence by disrupting *Campylobacter jejuni* phosphorylation signaling. *Cell Host Microbe* 2012;12:47–59.
33. Grasberger H, El-Zaatar M, Dang DT, Merchant JL. Dual oxidases control release of hydrogen peroxide by the gastric epithelium to prevent *Helicobacter felis* infection and inflammation in mice. *Gastroenterology* 2013;145:1045–1054.
34. Salonen A, Lahti L, Salojärvi J, et al. Impact of diet and individual variation on intestinal microbiota composition and fermentation products in obese men. *ISME J* 2014;8:2218–2230.
35. Lippert K, Kendenko L, Antonielli L, et al. Gut microbiota dysbiosis associated with glucose metabolism disorders and the metabolic syndrome in older adults. *Benef Microbes* 2017;8:545–556.
36. Zhou Q, Zhang Y, Wang X, et al. Gut bacteria *Akkermansia* is associated with reduced risk of obesity: evidence from the American Gut Project. *Nutr Metab (Lond)* 2020;17:90.
37. Wei YS, Hsiao Y-C, Su G-W, et al. Identification of hyperglycemia-associated microbiota alterations in saliva and gingival sulcus. *Arch Biochem Biophys* 2020;682:108278.
38. Renu S, Deblais L, Patil V, et al. Gut microbiota of obese children influences inflammatory mucosal immune pathways in the respiratory tract to influenza virus infection: optimization of an ideal duration of microbial colonization in a gnotobiotic pig model. *Microbiol Spectr* 2022;10:e0267421.
39. Karlsson CL, Karlsson CLJ, Onnerfält J, et al. The microbiota of the gut in preschool children with normal and excessive body weight. *Obesity (Silver Spring)* 2012;20:2257–2261.
40. Santacruz A, Collado MC, García-Valdés L, et al. Gut microbiota composition is associated with body weight, weight gain and biochemical parameters in pregnant women. *Br J Nutr* 2010;104:83–92.
41. Yassour M, Lim MY, Yun HS, et al. Sub-clinical detection of gut microbial biomarkers of obesity and type 2 diabetes. *Genome Med* 2016;8:17.
42. Parks BW, Nam E, Org E, et al. Genetic control of obesity and gut microbiota composition in response to high-fat, high-sucrose diet in mice. *Cell Metab* 2013;17:141–152.
43. Palleja A, Kashani A, Allin KH, et al. Roux-en-Y gastric bypass surgery of morbidly obese patients induces swift and persistent changes of the individual gut microbiota. *Genome Med* 2016;8:67.
44. Kostic AD, Gevers D, Siljander H, et al. The dynamics of the human infant gut microbiome in development and in progression toward type 1 diabetes. *Cell Host Microbe* 2015;17:260–273.
45. Shen F, Zheng R-D, Sun X-Q, et al. Gut microbiota dysbiosis in patients with non-alcoholic fatty liver disease. *Hepatobiliary Pancreat Dis Int* 2017;16:375–381.
46. Kootte RS, Levin E, Salojärvi J, et al. Improvement of insulin sensitivity after lean donor feces in metabolic syndrome is driven by baseline intestinal microbiota composition. *Cell Metab* 2017;26:611–619 e616.
47. Bajaj JS, Kassam Z, Fagan A, et al. Fecal microbiota transplant from a rational stool donor improves hepatic encephalopathy: a randomized clinical trial. *Hepatology* 2017;66:1727–1738.
48. Cani PD, Neyrinck AM, Maton N, Delzenne NM. Oligofructose promotes satiety in rats fed a high-fat diet: involvement of glucagon-like Peptide-1. *Obes Res* 2005;13:1000–1007.
49. Dong Z, Lv W, Zhang C, Chen S. Correlation analysis of gut microbiota and serum metabolome with porphyromonas gingivalis-induced metabolic disorders. *Front Cell Infect Microbiol* 2022;12:858902.
50. Forlano R, Mullish BH, Roberts LA, et al. The intestinal barrier and its dysfunction in patients with metabolic diseases and non-alcoholic fatty liver disease. *Int J Mol Sci* 2022;23:662.
51. Zhou ZY, Deng Y, Wen Y-L, et al. Chronic low-grade inflammation is involved in TLR4 knockout-induced spontaneous obesity in aged mice. *Biomed Pharmacother* 2022;147:112637.
52. Chitturi S, Farrell G, Frost L, et al. Serum leptin in NASH correlates with hepatic steatosis but not fibrosis: a manifestation of lipotoxicity? *Hepatology* 2002;36:403–409.
53. Knight ZA, Hannan KS, Greenberg ML, Friedman JM. Hyperleptinemia is required for the development of leptin resistance. *PLoS One* 2010;5:e11376.
54. Iizuka K, Takao K, Yabe D. ChREBP-mediated regulation of lipid metabolism: involvement of the gut microbiota,

- liver, and adipose tissue. *Front Endocrinol (Lausanne)* 2020;11:587189.
55. Begin-Heick N. Of mice and women: the beta 3-adrenergic receptor leptin and obesity. *Biochem Cell Biol* 1996;74:615–622.
 56. Wang CY, Liao JK. A mouse model of diet-induced obesity and insulin resistance. *Methods Mol Biol* 2012; 821:421–433.
 57. de Moura EDM, Dos Reis SA, da Conceição LL, et al. Diet-induced obesity in animal models: points to consider and influence on metabolic markers. *Diabetol Metab Syndr* 2021;13:32.
 58. Ghosh S, Whitley CS, Haribabu B, Jala VR. Regulation of intestinal barrier function by microbial metabolites. *Cell Mol Gastroenterol Hepatol* 2021;11:1463–1482.
 59. Freitag TL, Hartikainen A, Jouhten H, et al. Minor effect of antibiotic pre-treatment on the engraftment of donor microbiota in fecal transplantation in mice. *Front Microbiol* 2019;10:2685.
 60. Akiba Y, Maruta K, Takajo T, et al. Lipopolysaccharides transport during fat absorption in rodent small intestine. *Am J Physiol Gastrointest Liver Physiol* 2020; 318:G1070–G1087.
 61. Chomczynski P, Sacchi N. Single-step method of RNA isolation by acid guanidinium thiocyanate-phenol-chloroform extraction. *Anal Biochem* 1987;162:156–159.
 62. Livak KJ, Schmittgen TD. Analysis of relative gene expression data using real-time quantitative PCR and the 2⁻(delta delta C(T)) method. *Methods* 2001;25:402–408.
 63. Bamias G, Okazawa A, Rivera-Nieves J, et al. Commensal bacteria exacerbate intestinal inflammation but are not essential for the development of murine ileitis. *J Immunol* 2007;178:1809–1818.
 64. Wang F, Wang J, Liu D, Su Y. Normalizing genes for real-time polymerase chain reaction in epithelial and non-epithelial cells of mouse small intestine. *Anal Biochem* 2010;399:211–217.
 65. Yang YW, Chen M-K, Yang B-Y, et al. Use of 16S rRNA gene-targeted group-specific primers for real-time PCR analysis of predominant bacteria in mouse feces. *Appl Environ Microbiol* 2015;81:6749–6756.
 66. Petruska J, Goodman MF, Boosalis MS, et al. Comparison between DNA melting thermodynamics and DNA polymerase fidelity. *Proc Natl Acad Sci U S A* 1988; 85:6252–6256.
 67. Abu-Odeh M, Zhang Y, Reilly SM, et al. FGF21 promotes thermogenic gene expression as an autocrine factor in adipocytes. *Cell Rep* 2021;35:109331.
 68. Luo P, Wang F, Wong N-K, et al. Divergent roles of Kupffer cell TLR2/3 signaling in alcoholic liver disease and the protective role of EGCG. *Cell Mol Gastroenterol Hepatol* 2020;9:145–160.
 69. Pamir N, McMillen TS, Edgel KA, et al. Deficiency of lymphotoxin-alpha does not exacerbate high-fat diet-induced obesity but does enhance inflammation in mice. *Am J Physiol Endocrinol Metab* 2012;302:E961–E971.
 70. Truong DT, Franzosa EA, Tickle TL, et al. MetaPhlan2 for enhanced metagenomic taxonomic profiling. *Nat Methods* 2015;12:902–903.
 71. Abubucker S, Segata N, Goll J, et al. Metabolic reconstruction for metagenomic data and its application to the human microbiome. *PLoS Comput Biol* 2012;8: e1002358.
 72. Suzek BE, Huang H, McGarvey P, et al. UniRef: comprehensive and non-redundant UniProt reference clusters. *Bioinformatics* 2007;23:1282–1288.
 73. Kanehisa M, Goto S, Kawashima S, et al. The KEGG resource for deciphering the genome. *Nucleic Acids Res* 2004;32:D277–D280.
 74. Caspi R, Altman T, Dreher K, et al. The MetaCyc database of metabolic pathways and enzymes and the BioCyc collection of pathway/genome databases. *Nucleic Acids Res* 2012;40:D742–D753.
 75. McMurdie PJ, Holmes S. phyloseq: An R package for reproducible interactive analysis and graphics of microbiome census data. *PLoS One* 2013;8: e61217.
 76. Oksanen J, Blanchet G, Friendly M, Kindt R, Legendre P. *vegan: Community Ecology Package*; 2017.

Received May 24, 2022. Accepted June 13, 2023.

Correspondence

Address correspondence to: Maria T. Abreu, MD, Crohn's and Colitis Center, Division of Gastroenterology, Department of Medicine, University of Miami-Miller School of Medicine, PO Box 016960 (D-49), Miami, Florida 33101. e-mail: MAbreu1@med.miami.edu.

Acknowledgments

The authors would like to acknowledge the Onco-Genomics Shared Resource at the University of Miami Miller School of Medicine for performing the metagenomic sequencing of the microbiome. All schematics were created with BioRender.com. The graphical abstract was adapted from "Intestinal Infection Triggers Parkinson's Disease-like Symptoms in Pink1^{-/-} Mice," by BioRender.com.

All authors have reviewed and approved the manuscript.

CRedit Authorship Contributions

Hajar Hazime, MS (Conceptualization: Lead; Data curation: Lead; Formal analysis: Lead; Investigation: Lead; Methodology: Equal; Project administration: Supporting; Validation: Equal; Visualization: Lead; Writing – original draft: Lead; Writing – review & editing: Lead)

G. Michelle Ducasa, PhD (Conceptualization: Lead; Data curation: Lead; Formal analysis: Lead; Investigation: Lead; Methodology: Equal; Project administration: Supporting; Validation: Lead; Visualization: Lead; Writing – original draft: Equal; Writing – review & editing: Equal)

Anna Maribel M Santander (Resources: Lead)
 Nivis Brito (Methodology: Supporting)
 Eddy González, PhD (Data curation: Supporting)
 Yuguang Ban, PhD (Formal analysis: Supporting; Software: Equal)
 Jonathan Kaunitz, MD (Methodology: Supporting)
 Yasutada Akiba, PhD (Methodology: Supporting)
 Irina Fernandez, MS (Project administration: Lead)
 Juan F burgueno, DVM, PhD (Conceptualization: Lead; Writing – review & editing: Supporting)
 Maria T. Abreu, M.D. (Funding acquisition: Lead)

Conflicts of interest

This author discloses the following: Maria T. Abreu has served as a consultant to Boehringer Ingelheim Pharmaceuticals, Gilead, Janssen, AbbVie, Eli Lilly, and Landos Biopharma; serves as a trainer or lecturer for Imedex, Focus Medical Communications, and Cornerstones Health, Inc; and has funded projects by Pfizer, Prometheus Laboratories, and Takeda Pharmaceuticals. The remaining authors disclose no conflicts.

Funding

This work was supported by VA Merit Review Award I01BX001245 (J.D.K.), and grants from the National Institutes of Health, the National Institute of Diabetes and Digestive and Kidney Diseases (R01DK099076), the Micky & Madeleine Arison Family Foundation Crohn's & Colitis Discovery Laboratory, and Martin Kalsner Chair (M.A.).